

Study of the  $a_0(980)$  meson via the radiative decay  
 $\phi \rightarrow \eta\pi^0\gamma$  with the KLOE detector  
 KLOE Collaboration

F. Ambrosino<sup>e,f</sup>, A. Antonelli<sup>a</sup>, M. Antonelli<sup>a</sup>, F. Archilli<sup>j,k</sup>, C. Bacci<sup>l,m</sup>,  
 P. Beltrame<sup>b</sup>, G. Bencivenni<sup>a</sup>, S. Bertolucci<sup>a</sup>, C. Bini<sup>h,i</sup>, C. Bloise<sup>a</sup>,  
 S. Bocchetta<sup>l,m</sup>, F. Bossi<sup>a</sup>, P. Branchini<sup>m</sup>, P. Campana<sup>a</sup>, G. Capon<sup>a</sup>,  
 T. Capussela<sup>a</sup>, F. Ceradini<sup>l,m</sup>, S. Chi<sup>a</sup>, G. Chiefari<sup>e,f</sup>, P. Ciambrone<sup>a</sup>,  
 F. Crucianelli<sup>h</sup>, E. De Lucia<sup>a</sup>, A. De Santis<sup>h,i</sup>, P. De Simone<sup>a</sup>, G. De Zorzi<sup>h,i</sup>,  
 A. Denig<sup>b</sup>, A. Di Domenico<sup>h,i</sup>, C. Di Donato<sup>f</sup>, B. Di Micco<sup>l,m</sup>, A. Doria<sup>f</sup>,  
 M. Dreucci<sup>a</sup>, G. Felici<sup>a</sup>, A. Ferrari<sup>a</sup>, M. L. Ferrer<sup>a</sup>, S. Fiore<sup>h,i</sup>, C. Forti<sup>a</sup>,  
 P. Franzini<sup>h,i</sup>, C. Gatti<sup>a</sup>, P. Gauzzi<sup>\*,h,i</sup>, S. Giovannella<sup>a</sup>, E. Gorini<sup>c,d</sup>,  
 E. Graziani<sup>m</sup>, W. Kluge<sup>b</sup>, V. Kulikov<sup>p</sup>, F. Lacava<sup>h,i</sup>, G. Lanfranchi<sup>a</sup>,  
 J. Lee-Franzini<sup>a,n</sup>, D. Leone<sup>b</sup>, M. Martini<sup>a,g</sup>, P. Massarotti<sup>e,f</sup>, W. Mei<sup>a</sup>,  
 S. Meola<sup>e,f</sup>, S. Miscetti<sup>a</sup>, M. Moulson<sup>a</sup>, S. Müller<sup>a</sup>, F. Murtas<sup>a</sup>,  
 M. Napolitano<sup>e,f</sup>, F. Nguyen<sup>l,m</sup>, M. Palutan<sup>a</sup>, E. Pasqualucci<sup>i</sup>, A. Passeri<sup>m</sup>,  
 V. Patera<sup>a,g</sup>, F. Perfetto<sup>e,f</sup>, M. Primavera<sup>d</sup>, P. Santangelo<sup>a</sup>, G. Saracino<sup>e,f</sup>,  
 B. Sciascia<sup>a</sup>, A. Sciubba<sup>a,g</sup>, A. Sibidanov<sup>a</sup>, T. Spadaro<sup>a</sup>, M. Testa<sup>h,i</sup>,  
 L. Tortora<sup>m</sup>, P. Valente<sup>i</sup>, G. Venanzoni<sup>a</sup>, R. Versaci<sup>a,g</sup>, R. Volpe<sup>h,i</sup>, G. Xu<sup>a,o</sup>

<sup>a</sup>Laboratori Nazionali di Frascati dell'INFN, Via E.Fermi 40, I-00044 Frascati, Italy.

<sup>b</sup>Institut für Experimentelle Kernphysik, Universität Karlsruhe D-76128 Karlsruhe, Germany.

<sup>c</sup>Dipartimento di Fisica dell'Università del Salento, Via Arnesano, I-73100 Lecce, Italy.

<sup>d</sup>INFN Sezione di Lecce, Via Arnesano, I-73100 Lecce, Italy.

<sup>e</sup>Dipartimento di Scienze Fisiche dell'Università "Federico II", Via Cintia, I-80126 Napoli, Italy

<sup>f</sup>INFN Sezione di Napoli, Via Cintia, I-80126 Napoli, Italy

<sup>g</sup>Dipartimento di Energetica, Sapienza Università di Roma, P.le A.Moro, 2 I-00185 Roma, Italy.

<sup>h</sup>Dipartimento di Fisica, Sapienza Università di Roma, P.le A.Moro, 2 I-00185 Roma, Italy.

<sup>i</sup>INFN Sezione di Roma, P.le A.Moro, 2 I-00185 Roma, Italy.

<sup>j</sup>Dipartimento di Fisica dell'Università di Roma "Tor Vergata", Via della Ricerca Scientifica, 1 I-00133 Roma, Italy.

<sup>k</sup>INFN Sezione di Roma Tor Vergata, Via della Ricerca Scientifica, 1 I-00133 Roma, Italy.

<sup>l</sup>Dipartimento di Fisica dell'Università di Roma "Roma Tre", Via della Vasca Navale, 84 I-00146 Roma, Italy.

<sup>m</sup>INFN Sezione di Roma Tre, Via della Vasca Navale, 84 I-00146 Roma, Italy.

<sup>n</sup>Physics Department, State University of New York at Stony Brook, Stony Brook, NY 11794-3840 USA.

<sup>o</sup>Institute of High Energy Physics of Academica Sinica, PO Box 918 Beijing 100049, PR China.

<sup>p</sup>Institute for Theoretical and Experimental Physics, B. Cheremushkinskaya ul. 25, RU-117218 Moscow, Russia.

---

\*Corresponding author, Dipartimento di Fisica, Sapienza Università di Roma, P.le A.Moro, 2 I-00185 Roma, Italy; Tel. +390649914266, Fax +39064957697  
 Email address: paolo.gauzzi@roma1.infn.it (P. Gauzzi)

---

**Abstract**

We have studied the  $\phi \rightarrow a_0(980)\gamma$  process with the KLOE detector at the Frascati  $\phi$ -factory DAΦNE by detecting the  $\phi \rightarrow \eta\pi^0\gamma$  decays in the final states with  $\eta \rightarrow \gamma\gamma$  and  $\eta \rightarrow \pi^+\pi^-\pi^0$ . We have measured the branching ratios for both final states:  $Br(\phi \rightarrow \eta\pi^0\gamma) = (7.01 \pm 0.10 \pm 0.20) \times 10^{-5}$  and  $(7.12 \pm 0.13 \pm 0.22) \times 10^{-5}$  respectively. We have also extracted the  $a_0(980)$  mass and its couplings to  $\eta\pi^0$ ,  $K^+K^-$ , and to the  $\phi$  meson from the fit of the  $\eta\pi^0$  invariant mass distributions using different phenomenological models.

*Key words:*  $e^+e^-$  collisions, Scalar mesons, Rare  $\phi$  decays

*PACS:* 12.39.Mk, 13.20.Jf, 13.66.Bc, 14.40.Cs

---

**1. Introduction**

The problem of the internal structure of the scalar mesons with mass below 1 GeV is still open[1]. It is controversial whether they are  $q\bar{q}$  mesons[2],  $qq\bar{q}\bar{q}$  states[3], bound states of a  $K\bar{K}$  pair[4] or a mixing of these configurations.

An important part of the program of the KLOE experiment, carried out at the Frascati  $\phi$ -factory DAΦNE, has been dedicated to the study of the radiative decays  $\phi(1020) \rightarrow P_1P_2\gamma$  ( $P_{1,2}$  = pseudoscalar mesons). These decays are dominated by the exchange of a scalar meson  $S$  in the intermediate state ( $\phi \rightarrow S\gamma$ , and  $S \rightarrow P_1P_2$ ), and both their branching ratios and the  $P_1P_2$  invariant mass shapes depend on the scalar structure.

The  $\phi \rightarrow \eta\pi^0\gamma$  decay has been already used by KLOE and by other experiments to study the neutral component of the isotriplet  $a_0(980)$ [5, 6]. This process is well suited to study the  $\phi \rightarrow a_0(980)\gamma$  dynamics, since it is dominated by the scalar production, with small vector background, contrary to  $\pi^0\pi^0\gamma$  and  $\pi^+\pi^-\gamma$  cases, where a large irreducible background interferes with the  $f_0(980)$  signal[7]. In this paper the result of the analysis of the  $\phi \rightarrow \eta\pi^0\gamma$  decay, performed on a sample with 20 times larger statistics than the previously published paper[5], is presented. The final states corresponding to  $\eta \rightarrow \gamma\gamma$  and  $\eta \rightarrow \pi^+\pi^-\pi^0$  have been selected. The  $\eta\pi^0$  invariant mass distributions have been fit to two models of parametrization of the  $\phi \rightarrow a_0(980)\gamma$  decay, to extract the relevant  $a_0(980)$  parameters (mass and couplings).

**2. DAΦNE and KLOE**

The Frascati  $\phi$ -factory DAΦNE is an  $e^+e^-$  collider operating at a center of mass energy  $\sqrt{s} = M_\phi \simeq 1020$  MeV. The beams collide at an angle of  $(\pi - 0.025)$  rad, thus producing  $\phi$  mesons with small momentum ( $p_\phi \simeq 13$  MeV) in the horizontal plane. The KLOE detector[8] consists of two main subdetectors: a large volume drift chamber (DC) and a fine sampling lead-scintillating fibers electromagnetic calorimeter (EMC). The whole apparatus is inserted in a 0.52 T

axial magnetic field, produced by a superconducting coil. The DC is 3.3 m long, with inner and outer radii of 25 and 200 cm respectively. It contains 12 582 drift cells arranged in 58 stereo layers uniformly distributed in the sensitive volume and it is filled with a gas mixture of 90% helium and 10% isobutane. Its spatial resolution is 200  $\mu\text{m}$  and the tracks coming from the beam interaction point (IP) are reconstructed with  $\sigma(p_{\perp})/p_{\perp} \leq 0.4\%$ . The position resolution for two track vertices is about 3 mm.

The DC is surrounded by the EMC, that covers 98% of the solid angle, and is divided into a barrel, made of 24 trapezoidal modules about 4 m long, with the fibres running parallel to the barrel axis, and two endcaps of 32 modules each, with fibres aligned vertically. The read-out granularity is  $\sim 4.4 \times 4.4 \text{ cm}^2$ , for a total of 2440 cells, read at both ends by photomultipliers. The coordinate of a particle along the fiber direction is reconstructed from the difference of the arrival time of the signals at the two ends of the cell. Cells close in time and space are grouped together into clusters. The cluster energy is the sum of the cell energies, while the cluster time and position are energy weighted averages. The energy and time resolutions for photons are  $\sigma_E/E = 5.7\%/\sqrt{E(\text{GeV})}$  and  $\sigma_t = 57 \text{ ps}/\sqrt{E(\text{GeV})} \oplus 100 \text{ ps}$  respectively. Cluster positions are measured with resolutions of 1.3 cm in the coordinates transverse to the fibers, and 1.2  $\text{cm}/\sqrt{E(\text{GeV})}$  in the longitudinal coordinate. The detection efficiency for photons of  $E \simeq 20 \text{ MeV}$  is greater than 80% and reaches almost 100% at  $E > 80 \text{ MeV}$ .

The KLOE trigger is based on the detection of two energy deposits in the EMC, with  $E > 50 \text{ MeV}$  in the barrel and  $E > 150 \text{ MeV}$  in the endcaps.

### 3. Event selection

The results are based on the data collected during the 2001-02 run, at  $\sqrt{s} \simeq M_{\phi}$ . Of the two selected decay chains, the fully neutral one is characterized by high statistics and large background, while the charged one has small background but lower statistics. These two decay chains have been selected with different criteria and slightly different data samples have been used: 414  $\text{pb}^{-1}$  for the fully neutral and 383  $\text{pb}^{-1}$  for the charged decay. Monte Carlo (MC) samples of signal and of background processes have been produced with the simulation program of the experiment[9]. They have been generated on a run-by-run basis, simulating the machine operating conditions and background levels as measured in the data. Three MC samples, generated with different luminosity scale factors ( $\text{LSF} = L_{MC}/L_{data}$ ), have been used:

1. the *rad* sample contains all the radiative  $\phi$ -decays plus the non resonant process  $e^+e^- \rightarrow \omega\pi^0$ , with  $\text{LSF}=5$ ;
2. the *kk* sample contains  $\phi \rightarrow K^0\bar{K}^0$  with all subsequent kaon decays generated with  $\text{LSF}=1$ ;
3. the *all* sample contains all the  $\phi$  decays with  $\text{LSF}=1/5$ ; it is used to find possible backgrounds not included in the two main samples.

The shape of the  $\eta\pi^0$  invariant mass distribution has been simulated according to the spectrum obtained from the previously published analysis[5].

### 3.1. $\phi \rightarrow \eta\pi^0\gamma$ with $\eta \rightarrow \gamma\gamma$

This final state is characterized by five prompt photons originating from the IP. A prompt photon is defined as an EMC cluster not associated to any charged track in the DC and satisfying the condition  $|t - r/c| < \min[5\sigma_t(E), 2 \text{ ns}]$ , where  $t$  is the photon flight time,  $r$  is the corresponding path length, and  $c$  is the speed of light. Events with exactly five prompt clusters, with  $E > 3 \text{ MeV}$  and polar angle  $\vartheta > 21^\circ$  with respect to the beam line, are selected.

The main background originates from the other five photon final states,  $\phi \rightarrow f_0(980)\gamma \rightarrow \pi^0\pi^0\gamma$  and  $e^+e^- \rightarrow \omega\pi^0 \rightarrow \pi^0\pi^0\gamma$ , and from the seven photon process,  $\phi \rightarrow \eta\gamma$  with  $\eta \rightarrow 3\pi^0$ , which can mimic five photon events due to either photon loss or cluster merging. Also the three photon final states,  $\phi \rightarrow \eta(\pi^0)\gamma$  with  $\eta(\pi^0) \rightarrow \gamma\gamma$ , give a small contribution to the selected sample, when fake clusters are produced either by accidental coincidence with machine background or by cluster splittings. Other background processes are negligible.

The following analysis steps are then applied to the selected events.

1. First kinematic fit which imposes the total 4-momentum conservation and the speed of light for each photon, with 9 degrees of freedom. Events with  $\chi_{fit1}^2 > 27$  are rejected. A cut at 980 MeV on the total energy of the three most energetic photons is also applied to reject residual three photon events (processes 4 and 5 of Table 1).
2. Search for the best photon pairing to  $\eta$ 's and  $\pi^0$ 's, by choosing the combination that minimizes the  $\chi^2$ -like variable ( $i, j, k, l = 1, \dots, 5$  are the photon indices):

$$\chi_{pair}^2 = \frac{(M_{ij} - M_{P_1})^2}{\sigma_{M_{P_1}}^2} + \frac{(M_{kl} - M_{P_2})^2}{\sigma_{M_{P_2}}^2}$$

for both  $P_1P_2 = \eta\pi^0$  (signal) or  $\pi^0\pi^0$  (background) hypotheses.  $\sigma_{M_{\pi^0}}$  and  $\sigma_{M_\eta}$  are the width of the  $\pi^0$  and  $\eta$  peaks after the first kinematic fit ( $\sigma_{M_{\pi^0}} = 6 \text{ MeV}$  and  $\sigma_{M_\eta} = 9 \text{ MeV}$ ).

3. Second kinematic fit with the two additional constraints of the masses of the intermediate particles. The number of degrees of freedom is 11.

Background from process 1 and 3 of Table 1 dominates the tail of the distribution of the  $\chi_{fit2}^2$  of the second kinematic fit, as shown in Fig.1, and it can be reduced by cutting at  $\chi_{fit2}^2 < 24$ . By using the photon pairing in the background hypothesis,  $\pi^0\pi^0\gamma$ , the Dalitz plot of Fig.1 is obtained: the  $f_0\gamma$  background populates the lower right corner, while the two straight bands are the contribution of  $\omega\pi^0$ . The  $a_0$  signal is contained in the region between these bands. The  $\omega\pi^0$  background is strongly reduced by cutting out the two bands shown in Fig.1. Assuming the background hypothesis  $\omega\pi^0$ , the angle  $\theta^*$  between the non associated photon and the  $\omega$  flight direction can be defined. The regions at large  $|\cos\theta^*|$  (Fig.2.left) are dominated by  $\omega\pi^0$  and  $f_0\gamma$  backgrounds. The

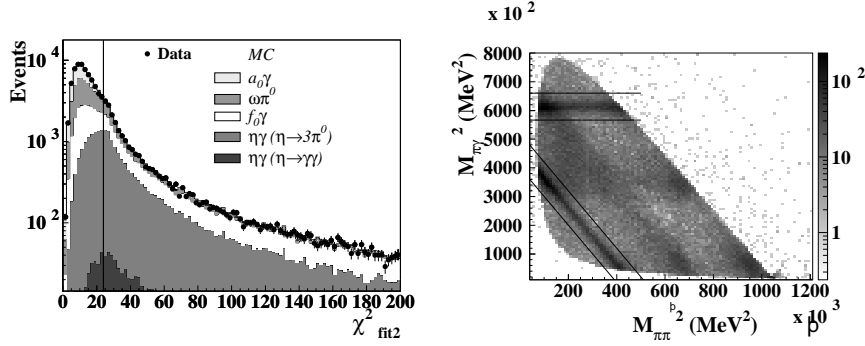


Figure 1: Right:  $\chi^2$  of the second kinematic fit; the applied cut at  $\chi^2_{fit2} = 24$  is also shown. Left: Dalitz plot of data in the background hypothesis ( $\pi^0\pi^0\gamma$ ).

cut  $|\cos\theta^*| < 0.8$  is then applied. Another effective cut to reduce the  $f_0\gamma$  background is  $\theta_{23} > 42^\circ$  (Fig.2.right), where  $\theta_{23}$  is the angle between the second and third photons ordered by decreasing energy.

After these cuts the overall selection efficiency, evaluated by MC, is almost independent from the  $\eta\pi^0$  invariant mass and its average value is 38.5%. The final

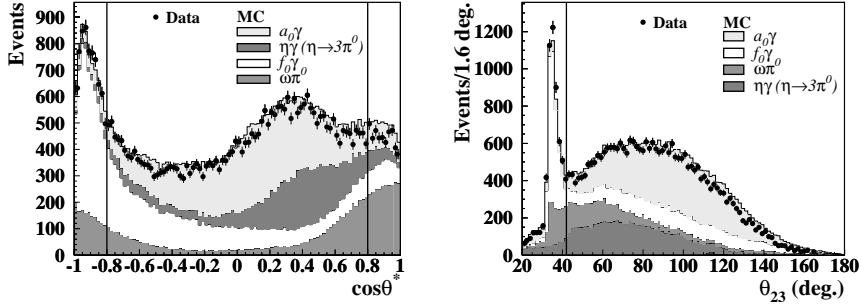


Figure 2: Left:  $\cos\theta^*$  distribution (see text for explanation); right: angle between the second and third photons ordered by decreasing energy (vertical lines represent the applied cuts).

sample consists of 29 601 events and the expected S/B ratio is about 1.0 (see Table 1). The residual background is irreducible and has to be evaluated and subtracted. A reweighing procedure has been adopted:

1. for each specific background process a data sample with a small signal content (below few percent) has been selected;
2. a fit has been performed on selected kinematical distributions, using the corresponding MC shapes to determine the weight to be assigned to that specific background; the weight is defined as the ratio of the number of events found by the fit to the number of expected events from MC.

In the last two columns of Table 1 the applied weights and the numbers of background events in the final sample are listed. The uncertainties are the com-

Table 1: Background processes for  $\phi \rightarrow \eta\pi^0\gamma$ , with  $\eta \rightarrow \gamma\gamma$ .  $(S/B)_1$  is the signal to background ratio after the preselection,  $(S/B)_2$  the same ratio at the end of the whole analysis chain. The reweighing factors,  $w$ , are also listed. Last column reports the final background estimate.

	Process	$(S/B)_1$	$(S/B)_2$	$w$	Background events
1	$\phi \rightarrow f_0\gamma \rightarrow \pi^0\pi^0\gamma$	0.40	4.4	1.2	$5062 \pm 60$
2	$e^+e^- \rightarrow \omega\pi^0 \rightarrow \pi^0\pi^0\gamma$	0.14	3.1	0.96	$3825 \pm 37$
3	$\phi \rightarrow \eta\gamma$ with $\eta \rightarrow 3\pi^0$	0.10	2.8	1.1	$7248 \pm 78$
4	$\phi \rightarrow \eta\gamma$ with $\eta \rightarrow \gamma\gamma$	1.6	200	2.5	$197 \pm 11$
5	$\phi \rightarrow \pi^0\gamma$	10	–	–	–
	Total background	0.05	1.0		$16\,332 \pm 86$

bination of MC statistics and of the systematics on the applied weights. The correlations have also been taken into account. After the background subtraction the number of signal event is  $13\,269 \pm 192$ . In Fig.3 the  $\eta\pi^0$  invariant mass distribution of the final sample is shown together with the background contributions. The invariant mass resolution is about 4 MeV, with non-gaussian tails mainly due to wrong photon combinations. In the same figure, the distribution of the polar angle  $\theta_{rec}$  of the recoil photon is plotted after the background subtraction: good agreement with the expected  $1 + \cos^2\theta_{rec}$  behaviour is shown.

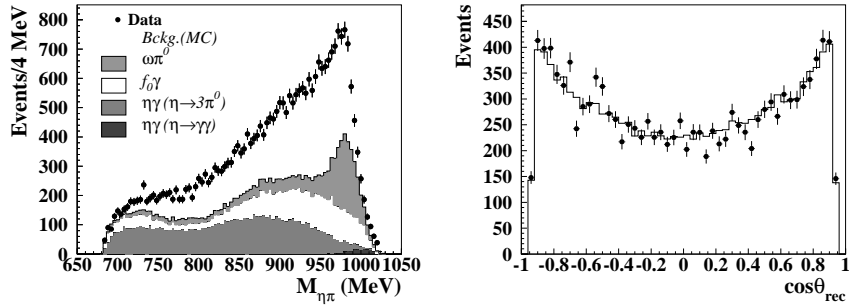


Figure 3: Left:  $\eta\pi^0$  invariant mass distribution of the neutral channel. Right: Distribution of the cosine of the polar angle of the recoil photon after background subtraction (dots), compared with the MC expectation (solid line).

### 3.2. $\phi \rightarrow \eta\pi^0\gamma$ with $\eta \rightarrow \pi^+\pi^-\pi^0$

With respect to the fully neutral one, this decay provides a lower statistics since the branching ratio of  $\eta \rightarrow \pi^+\pi^-\pi^0$  is smaller than for  $\eta \rightarrow \gamma\gamma$ . Moreover a lower acceptance is expected due to the larger number of particles to be

detected. However in this case there is a smaller background contamination, since no other final state with two tracks and five photons has a significant branching ratio from the  $\phi$ . The main sources of background are due to final states with two tracks and either four or six photons. In order of importance there are:  $e^+e^- \rightarrow \omega\pi^0$  with  $\omega \rightarrow \pi^+\pi^-\pi^0$  and a fake cluster;  $\phi \rightarrow K_S K_L$  with  $K_S \rightarrow \pi^+\pi^-$  and prompt  $K_L \rightarrow 3\pi^0$  with one photon lost;  $\phi \rightarrow K_S K_L$  with  $K_S \rightarrow \pi^0\pi^0$  and prompt  $K_L \rightarrow \pi^+\pi^-\pi^0$  or  $\pi\ell\nu$  with either one photon lost or one fake cluster;  $\phi \rightarrow \eta\gamma$  with  $\eta \rightarrow \pi^+\pi^-\pi^0$  plus two fake clusters.

The signal preselection requires the detection of two charged tracks and of five photons. The following requirements are then applied:

1. a vertex with two opposite sign tracks in a cylinder, around the IP, of 5 cm radius and 11 cm length;
2. five prompt photons with  $E > 10$  MeV;
3. total energy in the range  $900 < E_{tot} < 1160$  MeV and total momentum  $|\vec{P}_{tot}| < 110$  MeV/c;
4. the scalar sum of the momenta of the two pions  $P_\Sigma = |\vec{p}_1| + |\vec{p}_2|$ , outside the range  $418 < P_\Sigma < 430$  MeV/c, which identifies events with  $K_S \rightarrow \pi^+\pi^-$ .

Events surviving this preselection go to the kinematic fit stage, similar to that of the neutral channel.

1. A kinematic fit with 9 degrees of freedom is performed by imposing only the total 4-momentum conservation and speed of light for the photons; events with  $\chi_{fit1}^2 < 17$  are retained.
2. Photons are combined to build  $\pi^0$ 's and  $\eta$ 's. There are 15 possibilities to get two  $\pi^0$ 's out of five photons. For each of them there are two choices in the association of one  $\pi^0$  to the  $\pi^+\pi^-$  pair. For each of these 30 combinations  $\chi_{pair}^2$  is computed according to ( $i, j, k, l = 1, \dots, 5$  are the photon indices):

$$\chi_{pair}^2 = \frac{(M_{ij} - M_{\pi^0})^2}{\sigma_{M_{\pi^0}}^2} + \frac{(M_{kl} - M_{\pi^0})^2}{\sigma_{M_{\pi^0}}^2} + \frac{(M_{\pi^+\pi^-\pi^0} - M_\eta)^2}{\sigma_{M_\eta}^2}$$

Events with at least one combination with  $\chi_{pair}^2 < 10$  are retained.

3. The second kinematic fit is performed on all the combinations selected by the previous step adding the three mass constraints, for a total of 12 degrees of freedom. The combination with the lowest  $\chi_{fit2}^2$  is chosen. Only events with  $\chi_{fit2}^2 < 20$  are retained.
4. Finally, events with the recoil photon energy below 20 MeV are discarded to remove events with a spurious low energy photon.

The final sample consists of 4181 events. The overall selection efficiency for the signal, evaluated by MC, is 19.4%, almost independent from the  $\eta\pi^0$  invariant mass, decreasing only at very high invariant mass values. Fig.4 shows the data-MC agreement for the  $\chi^2$  distributions of the first and second kinematic fits. The MC distributions include signal and background events. The mass

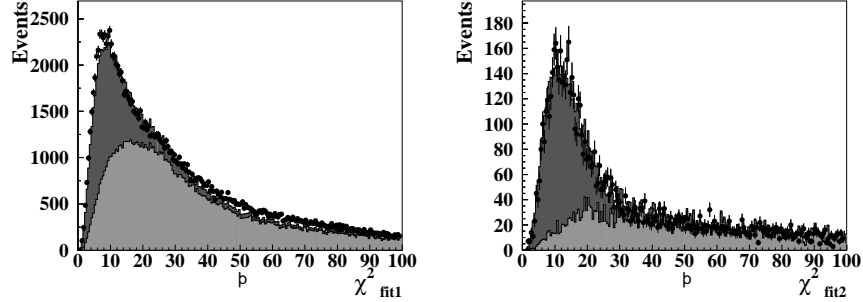


Figure 4:  $\chi^2$  distributions for the first (left) and second (right) kinematic fit. The selected data sample (points) is compared to the MC expectation (dark grey histograms) given by the weighed sum of the signal and the estimated background (light grey histograms).

resolution is about 4 MeV for all mass values, with non gaussian tails, mainly due to events with a wrong photon combination.

The residual background is evaluated by applying the selection procedure on MC samples and by checking the absolute normalization on background enriched data control samples. In order to properly normalize the observed numbers of events, data and MC samples after the preselection but before the kinematic fit have been used. At this level the expected contribution of the signal does not exceed  $2 \div 3\%$ . Four variables have been chosen to compare data and MC samples:  $E_{tot}$ ,  $|P_{tot}^x|$ ,  $M_{\gamma\gamma}$  and  $M_{\pi\pi\gamma\gamma}$  where  $M_{\gamma\gamma}$  is the invariant mass of any pair of photons (10 combinations per event) and  $M_{\pi\pi\gamma\gamma}$  is the invariant mass of the two pions and any pair of two photons (again 10 combinations per event). The four distributions for the data are simultaneously fit with the weighed sum of the same MC distributions for each background sample and for the signal. The weights of the *rad* and *kk* samples are the free parameters.  $w_{rad} = 0.45$  and  $w_{kk} = 1.3$  are obtained, from which the numbers of background events  $B_{rad} = 307$  and  $B_{kk} = 264$  are estimated. 8 additional background events from the *all* sample have also to be taken into account. The fit has been repeated separately on each control distribution and the spread obtained in the estimated number of events is taken as systematic uncertainty. The total number of background events is  $579 \pm 27$ , where the uncertainty is the quadratic sum of the statistical and the systematic uncertainties. This background accounts for about 14% of the selected events.

Fig.5 shows the  $\eta\pi^0$  invariant mass distribution. In the same figure, the distribution of the polar angle of the recoil photon is shown, and is compared to the MC expected behaviour. Also in this case the distribution agrees with the  $1 + \cos^2 \theta_{rec}$  dependence of the signal.



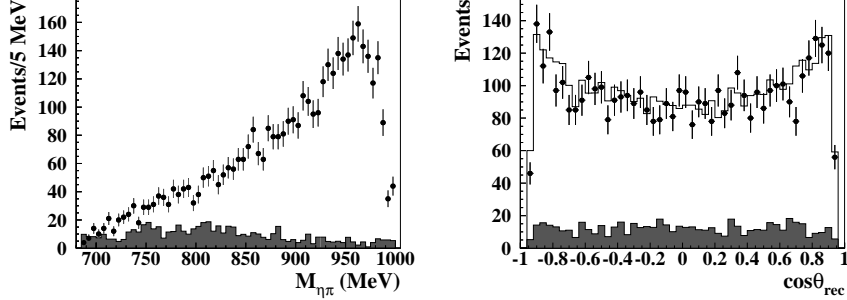


Figure 5: Left:  $\eta\pi^0$  invariant mass distribution for the final data sample (points) compared to the estimated background (dark histogram). Right: polar angle of the recoil photon for data (points) and for MC expectations (histogram). Dark histogram represents the background.

### 3.3. Branching ratio evaluation

The branching ratio of the process  $\phi \rightarrow \eta\pi^0\gamma$  is obtained from the formula:

$$Br(\phi \rightarrow \eta\pi^0\gamma) = \frac{N_f - B_f}{\varepsilon_f N_\phi^{(f)} Br(\eta \rightarrow f)} \quad (f = \gamma\gamma, \pi^+\pi^-\pi^0) \quad (1)$$

where  $N_f$  is the total number of selected events,  $B_f$  the estimated background,  $\varepsilon_f$  is the average efficiency.  $N_\phi$  is the number of produced  $\phi$  mesons evaluated from the number  $N_{\eta\gamma}$  of  $\phi \rightarrow \eta\gamma$  with  $\eta \rightarrow \pi^0\pi^0\pi^0$  events.

$$N_\phi = \frac{N_{\eta\gamma}}{\varepsilon_{\eta\gamma} Br(\phi \rightarrow \eta\gamma) Br(\eta \rightarrow \pi^0\pi^0\pi^0)} \quad (2)$$

The  $Br(\pi^0 \rightarrow \gamma\gamma)$  is not included in eq.(1) and (2) since it has been already taken into account in the MC. The normalization sample has been selected by requiring no tracks in the DC and six or more prompt clusters in the EMC, in the same runs used for the signal selection.  $N_{\eta\gamma} = 4.2 \times 10^6$  events have been found in the sample used for the analysis of the fully neutral decay chain, with efficiency  $\varepsilon_{\eta\gamma} = 81\%$ , corresponding to  $N_\phi^{(\gamma\gamma)} = (1.24 \pm 0.03) \times 10^9$ .

By using  $Br(\eta \rightarrow \gamma\gamma) = (39.31 \pm 0.20)\%$ [10], the branching ratio is obtained:

$$Br(\phi \rightarrow \eta\pi^0\gamma) = (7.01 \pm 0.10 \pm 0.20) \times 10^{-5} \quad (3)$$

The first uncertainty is due to statistics and to the background subtraction. Several sources of systematics have been taken into account (see Table 2): photon counting (dominated by the detection efficiency for low energy photons), the data-MC discrepancies in the evaluation of the selection efficiency, and the normalization uncertainty.

The data sample analyzed for the charged decay channel is slightly smaller than the other one,  $N_\phi^{(\pi^+\pi^-\pi^0)} = (1.15 \pm 0.03) \times 10^9$ . By using  $Br(\eta \rightarrow \pi^+\pi^-\pi^0) = (22.73 \pm 0.28)\%$ [10]

$$Br(\phi \rightarrow \eta\pi^0\gamma) = (7.12 \pm 0.13 \pm 0.22) \times 10^{-5} \quad (4)$$

Table 2: Main sources of systematic uncertainty on the branching ratio (3).

Source	uncert. ( $\times 10^{-5}$ )
Photon counting	0.08
Selection efficiency	0.12
$Br(\eta \rightarrow \gamma\gamma)$	0.04
$Br(\phi \rightarrow \eta\gamma)$	0.13
$Br(\eta \rightarrow \pi^0\pi^0\pi^0)$	0.05

is obtained. The first uncertainty is the quadratic sum of the statistical uncertainty on  $N_{\pi^+\pi^-\pi^0}$  and of the uncertainty on the background; the second one is systematic, mainly due to the absolute normalization, and includes a 1% error due to the efficiency evaluation.

The two branching ratios (3) and (4) are compatible with the old KLOE results:  $(8.51 \pm 0.51 \pm 0.57) \times 10^{-5}$  ( $\eta \rightarrow \gamma\gamma$ ) and  $(7.96 \pm 0.60 \pm 0.40) \times 10^{-5}$  ( $\eta \rightarrow \pi^+\pi^-\pi^0$ )[5]. By combining the two results, taking into account the common normalization error

$$Br(\phi \rightarrow \eta\pi^0\gamma) = (7.06 \pm 0.22) \times 10^{-5} \quad (5)$$

is obtained, where the uncertainty is both statistic and systematic.

#### 4. Fit of the $\eta\pi^0$ invariant mass distributions

In order to extract the relevant parameters of the  $a_0$ , a simultaneous fit, with the same set of free parameters, has been performed on the two  $\eta\pi^0$  invariant mass distributions, by minimizing the following  $\chi^2$ :

$$\chi^2 = \sum_{f=\gamma\gamma, \pi^+\pi^-\pi^0} \sum_{i=1}^{n_f} \frac{(N_i^{(f)} - B_i^{(f)} - E_i^{(f)})^2}{\sigma_i^{(f)2}}$$

where  $n_f$  is the number of bins of respectively the fully neutral and charged  $\eta\pi^0$  mass distribution;  $N_i$  is the content of the  $i$ -th bin and  $B_i$  is the number of background events to be subtracted from the  $i$ -th bin. The expected number of events,  $E_i$ , can be written as

$$E_i^{(f)} = N_\phi^{(f)} \sum_{j=1}^{n_f} \varepsilon_{ij}^{(f)} \frac{1}{\Gamma_\phi} \int_{\text{bin } j} \frac{d\Gamma_{th}(\phi \rightarrow \eta\pi^0\gamma)}{dm} dm \times Br(\eta \rightarrow f)$$

where  $m = M_{\eta\pi^0}$ , and  $\Gamma_\phi = 4.26$  MeV[10].  $\varepsilon_{ij}^{(f)}$  is the efficiency matrix (also referred to as smearing matrix), representing the probability of a signal event with “true” mass in the  $j$ -th bin of the spectrum to be reconstructed in the  $i$ -th bin. The efficiency matrices, evaluated by MC, are almost diagonal; the off-diagonal elements take into account resolution effects as well as wrong photon

pairings. The differential decay width  $d\Gamma_{th}/dm$  has been parametrized according to two different models.

In the ‘‘Kaon Loop’’ (KL) model[11] the  $\phi$  is coupled to the scalar meson through a loop of charged kaons. The theoretical function can be written as:

$$\frac{d\Gamma_{th}(\phi \rightarrow \eta\pi^0\gamma)}{dm} = \frac{d\Gamma_{scal}}{dm} + \frac{d\Gamma_{vect}}{dm} + \frac{d\Gamma_{interf}}{dm} \quad (6)$$

The scalar term  $d\Gamma_{scal}/dm$  is described in some details in Appendix A.  $d\Gamma_{vect}/dm$ , is dominated by  $\phi \rightarrow \rho\pi^0$  with  $\rho \rightarrow \eta\gamma$  and is described in the framework of the Vector Dominance Models (VDM)[12]. Last term is the interference between the scalar and the vector amplitudes.

The free fit parameters are: the  $a_0$  mass, the couplings  $g_{a_0K^+K^-}$ ,  $g_{a_0\eta\pi^0}$ , the branching ratio of the vector contribution, the relative phase  $\delta$  between scalar and vector amplitudes, and, as a relative normalization between the two different final states, the ratio  $R_\eta = Br(\eta \rightarrow \gamma\gamma)/Br(\eta \rightarrow \pi^+\pi^-\pi^0)$ .

An alternative parametrization of the amplitude of the decay  $\phi \rightarrow \eta\pi^0\gamma$  has been also used, following ref.[13]. A point-like coupling of the scalar to the  $\phi$  meson is assumed, hence this model will be called ‘‘No Structure’’ (NS) in the following. The scalar meson is parametrized as a Breit-Wigner interfering with a polynomial scalar background and with a vector background (see Appendix B). The free parameters in this case are the couplings  $g_{a_0K^+K^-}$ ,  $g_{a_0\eta\pi^0}$ , and  $g_{\phi a_0\gamma}$ , the ratio  $R_\eta$ , the branching ratio of the vector background, and two complex coefficients,  $b_0$  and  $b_1$ , of the scalar background. The  $a_0$  mass is fixed to avoid fit instabilities, due the large number of free parameters, and due to the large cancellations that occur among the terms of eq.(9). The chosen value of the  $a_0$  mass is the result of the KL fit.

The fit results are shown in Fig.6, and the parameter values are listed in

Table 3: Fit results for KL and NS models.

	KL	NS
$M_{a_0}$ (MeV)	$982.5 \pm 1.6 \pm 1.1$	982.5 (fixed)
$g_{a_0K^+K^-}$ (GeV)	$2.15 \pm 0.06 \pm 0.06$	$2.01 \pm 0.07 \pm 0.28$
$g_{a_0\eta\pi^0}$ (GeV)	$2.82 \pm 0.03 \pm 0.04$	$2.46 \pm 0.08 \pm 0.11$
$g_{\phi a_0\gamma}$ (GeV <sup>-1</sup> )		$1.83 \pm 0.03 \pm 0.08$
$\delta$ (deg.)	$222 \pm 13 \pm 3$	
B.r. of vector backg. ( $\times 10^6$ )	$0.92 \pm 0.40 \pm 0.15$	$\sim 0$
$R_\eta$	$1.70 \pm 0.04 \pm 0.03$	$1.70 \pm 0.03 \pm 0.01$
$ b_0 $		$14.9 \pm 0.6 \pm 0.5$
$arg(b_0)$ (deg.)		$38.3 \pm 1.1 \pm 0.6$
$ b_1 $		$21.3 \pm 1.4 \pm 0.9$
$arg(b_1)$ (deg.)		$57.3 \pm 1.4 \pm 1.1$
$\chi^2/ndf$	157.1 / 136	140.6 / 133
$P(\chi^2)$	10.4%	30.9%

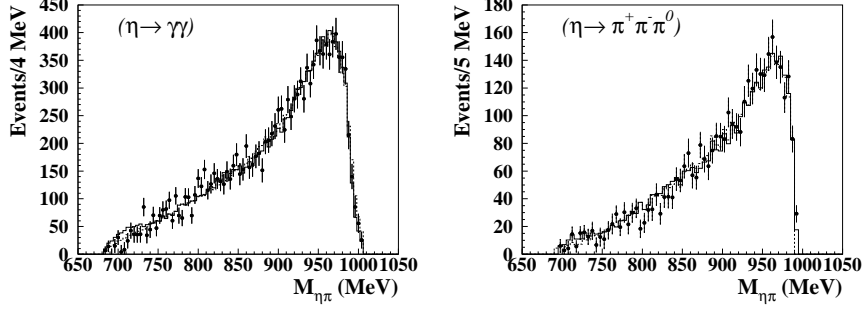


Figure 6: Fit results: points are data after background subtraction; histograms represent the fit functions for KL (solid) and NS (dashed) models.

Table 4: Correlation coefficients among the relevant  $a_0$  parameters.

KL model				NS model			
	$M_{a_0}$	$g_{a_0 K^+ K^-}$	$g_{a_0 \eta \pi^0}$		$g_{a_0 K^+ K^-}$	$g_{a_0 \eta \pi^0}$	$g_{\phi a_0 \gamma}$
$M_{a_0}$	1.			$g_{a_0 K^+ K^-}$	1.		
$g_{a_0 K^+ K^-}$	0.931	1.		$g_{a_0 \eta \pi^0}$	-0.565	1.	
$g_{a_0 \eta \pi^0}$	0.584	0.550	1.	$g_{\phi a_0 \gamma}$	-0.138	0.657	1.

Table 3. Good  $\chi^2$  probability is obtained for both models.

The ratio  $R_\eta$  is in good agreement with the PDG value  $1.729 \pm 0.028$ [10], confirming that the two samples are consistent with each other.

A vector background smaller than the VDM predictions,  $(3 \div 5) \times 10^{-6}$ [12, 15], is found in both fits, indicating that the  $\phi \rightarrow \eta \pi^0 \gamma$  process is largely dominated by  $\phi \rightarrow a_0 \gamma$ .

In the KL case, the  $a_0$  mass is in agreement with the PDG value  $(985.1 \pm 1.3)$  MeV[10]. A ratio of the squared coupling constants  $R_{a_0} = g_{a_0 K^+ K^-}^2 / g_{a_0 \eta \pi^0}^2 = 0.58 \pm 0.03 \pm 0.03$  can be derived. The  $g_{\phi a_0 \gamma}$  is not a free parameter of this model, but can be obtained according to the formula:

$$\begin{aligned}
 g_{\phi a_0 \gamma} &= \sqrt{\frac{3}{\alpha} \left( \frac{2M_\phi}{M_\phi^2 - M_{a_0}^2} \right)^3 \Gamma_\phi Br(\phi \rightarrow \eta \pi^0 \gamma)} = \\
 &= 1.58 \pm 0.10 \pm 0.16 \text{ GeV}^{-1}
 \end{aligned}
 \tag{7}$$

The  $a_0$  width obtained from eq.(8) is  $\Gamma_{a_0}(M_{a_0}) \simeq 105$  MeV.

In Table 4 the correlation coefficients among the  $a_0$  parameters are shown.

The couplings  $g_{a_0 K^+ K^-}$  and  $g_{a_0 \eta \pi^0}$  of the NS fit and therefore the ratio  $R_{a_0} = 0.67 \pm 0.06 \pm 0.13$  are in agreement with the KL values. In the NS case  $g_{\phi a_0 \gamma}$  can be determined directly and is compatible with the value of eq.(7). From

this fit a total decay width  $\Gamma_{a_0}(M_{a_0}) \simeq 80$  MeV can be evaluated according to eq.(10).

The systematic uncertainties on the parameters account for: (i) sensitivity to the fixed parameters (the  $a_0$  coupling to  $\eta'\pi^0$ ,  $g_{a_0\eta'\pi^0}$ , and  $g_{\phi K^+K^-}$  in the KL model,  $M_{a_0}$  in the NS model); (ii) normalization uncertainty; (iii) data-MC discrepancy of the fraction of wrong photon pairings (12% from data and 14% from MC).

## 5. Unfolding of the $\eta\pi^0$ invariant mass distribution

In order to allow a better comparison with other experimental results and with theoretical models, the invariant mass distribution should be corrected for resolution and smearing effects. Therefore an unfolding procedure has been applied to the  $\eta\pi^0$  invariant mass distributions by using the method described in ref.[16]. This is an iterative procedure based on the Bayes theorem, which does not require the inversion of the smearing matrix.

The unfolding has been performed separately on both invariant mass distributions before the background subtraction. The smearing matrices are the same used in the fits described in Sect.4.

An initial distribution has to be provided as starting point of the iterative procedure; the unfolded distributions obtained starting from the output of the KL fit or from a flat distribution in  $M_{\eta\pi^0}$  differ by less than 3%. This difference has been taken into account in the uncertainty evaluation.

The bin by bin average of the two unfolded distributions is used to calculate the differential branching ratio  $(1/\Gamma_\phi)(d\Gamma(\phi \rightarrow \eta\pi^0\gamma)/dM_{\eta\pi^0})$  reported in Table 5. The uncertainties are both from statistics (data and MC) and from systematics. The main contribution to the systematic error is the difference between the two unfolded distributions. The correlation of the contents of nearest neighbour bins of invariant mass is about 50%, for next-nearest neighbour bins is about 20%, and is negligible for bin distance greater than two.

An additional uncertainty of 3% on the absolute scale has to be considered, according to eq.(5).

To check this procedure, the unfolded distribution has been fit to the KL model, without requiring any smearing matrix. The parameters values are in good agreement with those of Table 3.

## 6. Conclusions

A high statistics study of the process  $\phi \rightarrow \eta\pi^0\gamma$  has been performed, by selecting the decay chains corresponding to  $\eta \rightarrow \gamma\gamma$  and  $\eta \rightarrow \pi^+\pi^-\pi^0$ .

$Br(\phi \rightarrow \eta\pi^0\gamma) = (7.01 \pm 0.10 \pm 0.21) \times 10^{-5}$  and  $(7.12 \pm 0.13 \pm 0.22) \times 10^{-5}$  respectively have been measured.

A simultaneous fit of the two invariant mass distributions has been performed, which shows that the two samples are consistent with each other.

Table 5: Differential branching ratio:  $m$  is the bin center, the errors are the total uncertainties, and the bin width is 6.35 MeV.

$m$ (MeV)	$(1/\Gamma_\phi)(d\Gamma_{\eta\pi^0\gamma}/dm) \times 10^7$ (MeV $^{-1}$ )	$m$ (MeV)	$(1/\Gamma_\phi)(d\Gamma_{\eta\pi^0\gamma}/dm) \times 10^7$ (MeV $^{-1}$ )
691.53	0.06 $\pm$ 0.07	850.35	2.25 $\pm$ 0.13
697.88	0.18 $\pm$ 0.10	856.71	2.35 $\pm$ 0.14
704.24	0.18 $\pm$ 0.12	863.06	2.27 $\pm$ 0.13
710.59	0.31 $\pm$ 0.13	869.41	2.35 $\pm$ 0.13
716.94	0.30 $\pm$ 0.08	875.76	2.42 $\pm$ 0.16
723.29	0.38 $\pm$ 0.11	882.12	2.59 $\pm$ 0.16
729.65	0.53 $\pm$ 0.17	888.47	2.80 $\pm$ 0.14
736.00	0.51 $\pm$ 0.13	894.82	2.92 $\pm$ 0.19
742.35	0.53 $\pm$ 0.05	901.18	3.18 $\pm$ 0.20
748.71	0.67 $\pm$ 0.07	907.53	3.37 $\pm$ 0.17
755.06	0.81 $\pm$ 0.07	913.88	3.48 $\pm$ 0.17
761.41	0.94 $\pm$ 0.10	920.24	3.67 $\pm$ 0.17
767.76	0.99 $\pm$ 0.11	926.59	3.94 $\pm$ 0.17
774.12	0.99 $\pm$ 0.08	932.94	4.29 $\pm$ 0.25
780.47	1.08 $\pm$ 0.09	939.29	4.63 $\pm$ 0.25
786.82	1.30 $\pm$ 0.10	945.65	4.89 $\pm$ 0.21
793.18	1.27 $\pm$ 0.13	952.00	5.20 $\pm$ 0.22
799.53	1.42 $\pm$ 0.28	958.35	5.40 $\pm$ 0.28
805.88	1.63 $\pm$ 0.28	964.71	5.44 $\pm$ 0.33
812.24	1.71 $\pm$ 0.14	971.06	5.35 $\pm$ 0.22
818.59	1.79 $\pm$ 0.16	977.41	4.94 $\pm$ 0.21
824.94	1.66 $\pm$ 0.18	983.76	4.02 $\pm$ 0.19
831.29	1.82 $\pm$ 0.15	990.12	2.80 $\pm$ 0.27
837.65	1.96 $\pm$ 0.12	996.47	1.51 $\pm$ 0.32
844.00	2.13 $\pm$ 0.13		

Both models used in the fits, the  $\phi$ -scalar meson coupling through the kaon loop (KL model) and the direct coupling (NS model), are able to reproduce the experimental  $\eta\pi^0$  mass distribution.

From the fit results that  $\phi \rightarrow \eta\pi^0\gamma$  decay is dominated by  $\phi \rightarrow a_0(980)\gamma$ , since the vector contribution is very small,  $Br(e^+e^- \rightarrow VP \rightarrow \eta\pi^0\gamma) < 10^{-6}$ .

The fit allows also the extraction of the  $a_0(980)$  mass and its couplings to  $\eta\pi^0$ ,  $K^+K^-$ , and to the  $\phi$  meson. The mass agrees at one standard deviation level with the PDG value. The two sets of couplings obtained from the fits agree with each other. Using these couplings, a total decay width of the  $a_0(980)$  in the range  $80 \div 105$  MeV is estimated. The ratio  $R_{a_0} = g_{a_0K^+K^-}^2 / g_{a_0\eta\pi^0}^2 \simeq 0.6 - 0.7$  is obtained. A large  $g_{\phi a_0\gamma}$  has been found ( $1.6 \div 1.8$  GeV $^{-1}$ ) suggesting a sizeable strange quark content of the  $a_0(980)$ .

## 7. Acknowledgments

We thank the DAΦNE team for their efforts in maintaining low background running conditions and their collaboration during all data-taking. We want to thank our technical staff: G. F. Fortugno and F. Sborzacchi for their dedicated work to ensure an efficient operation of the KLOE Computing Center; M. Anelli for his continuous support to the gas system and the safety of the detector; A. Balla, M. Gatta, G. Corradi, and G. Papalino for the maintenance of the electronics; M. Santoni, G. Paoluzzi, and R. Rosellini for the general support to the detector; C. Piscitelli for his help during major maintenance periods. This work was supported in part by EURODAΦNE, contract FMRX-CT98-0169; by the German Federal Ministry of Education and Research (BMBF) contract 06-KA-957; by the German Research Foundation (DFG), 'Emmy Noether Programme', contracts DE839/1-4; by INTAS, contracts 96-624, 99-37; and by the EU Integrated Infrastructure Initiative HadronPhysics Project under contract number RII3-CT-2004-506078.

### A. Appendix: main formulas of the KL model[11]

The scalar term of eq.(6) has the form:

$$\frac{d\Gamma_{scal}}{dm} = \frac{2|g_{\phi K^+K^-} - g(m)|^2 p_{\eta\pi^0} (M_\phi^2 - m^2)}{3(4\pi)^2 M_\phi^3} \left| \frac{g_{a_0 K^+K^-} - g_{a_0 \eta\pi^0}}{D_{a_0}(m)} \right|^2$$

where

$$p_{\eta\pi^0} = \frac{\sqrt{[m^2 - (M_\eta - M_{\pi^0})^2][m^2 - (M_\eta + M_{\pi^0})^2]}}{2m}$$

The detailed formulation of the KL function  $g(m)$  can be found in ref.[11].  $D_{a_0}(m)$  is the inverse propagator of the  $a_0$ :

$$D_{a_0}(m) = M_{a_0}^2 - m^2 + \sum_{ab} [Re\Pi_{ab}(M_{a_0}) - \Pi_{ab}(m)]$$

The sum is extended over all the possible two particle decays of the  $a_0$ :  $ab = \eta\pi^0$ ,  $K^+K^-$ ,  $K^0\bar{K}^0$ , and  $\eta'\pi^0$ .

The  $a_0$  width is:

$$\Gamma_{a_0}(m) = \frac{\sum_{ab} Im\Pi_{ab}(m)}{m} = \frac{\sum_{ab} g_{a_0 ab}^2 \rho_{ab}(m)}{16\pi m} \quad (8)$$

where:

$$\rho_{ab}(m) = \sqrt{\left(1 - \frac{(m_a + m_b)^2}{m^2}\right) \left(1 - \frac{(m_a - m_b)^2}{m^2}\right)}$$

The parameters of the scalar term that are determined by the fit are the  $a_0$  mass and the couplings  $g_{a_0 K^+K^-}$  and  $g_{a_0 \eta\pi^0}$ . The  $a_0$  to  $\eta'\pi^0$  coupling is fixed either to  $g_{a_0 \eta'\pi^0} = -\sqrt{2} \cos\varphi_P g_{a_0 K^+K^-}$  ( $qq\bar{q}\bar{q}$  hypothesis) or to  $g_{a_0 \eta'\pi^0} =$

$2 \sin\varphi_P g_{a_0 K^+ K^-}$  ( $q\bar{q}$  hypothesis), where  $\varphi_P$  is the pseudoscalar mixing angle (the value  $\varphi_P = 39.7^\circ$  has been used[17]). Another fixed parameter is the coupling of the  $\phi$  to the  $K^+ K^-$  pair:

$$g_{\phi K^+ K^-} = \frac{M_\phi \sqrt{48\pi Br(\phi \rightarrow K^+ K^-)} \Gamma_\phi}{(M_\phi^2 - 4M_K^2)^{3/4}} = 4.49 \pm 0.07$$

## B. Appendix: main formulas of the NS model[13]

The differential decay width of the NS model is the following:

$$\begin{aligned} \frac{d\Gamma_{th}(\phi \rightarrow \eta\pi^0\gamma)}{dm} &= \frac{8\pi\alpha p_{\eta\pi^0} (M_\phi^2 - m^2)^3}{3 M_\phi^3} \left| \frac{g_{\phi a_0 \gamma} g_{a_0 \eta\pi^0}}{m^2 - M_{a_0}^2 + iM_{a_0}\Gamma_{a_0}(m)} + \right. \\ &\quad \left. + \frac{b_0}{M_\phi^2} + \frac{b_1}{M_\phi^4} (m^2 - M_{a_0}^2) + A_{vect} \right|^2 \end{aligned} \quad (9)$$

The resonance width is mass dependent according to ref.[14]:

$$\Gamma_{a_0}(m) = \Gamma_{\eta\pi^0}(m) + \Gamma_{K^+ K^-}(m) + \Gamma_{K^0 \bar{K}^0}(m)$$

$$\text{where : } \Gamma_{\eta\pi^0}(m) = \frac{g_{a_0 \eta\pi^0}^2}{8\pi m^2} p_{\eta\pi^0};$$

$$\Gamma_{K\bar{K}}(m) = \frac{g_{a_0 K^+ K^-}^2}{16\pi m} \sqrt{1 - (2M_K/m)^2} \quad \text{for } m > 2M_K; \quad (10)$$

$$\Gamma_{K\bar{K}}(m) = \frac{ig_{a_0 K^+ K^-}^2}{16\pi m} \sqrt{(2M_K/m)^2 - 1} \quad \text{for } m < 2M_K$$

$$\text{(with } K\bar{K} = K^+ K^-, K^0 \bar{K}^0)$$

The scalar background is parametrized with a polynomial with two complex coefficients,  $b_0$  and  $b_1$ . The vector background,  $A_{vect}$ , takes into account all processes  $e^+ e^- \rightarrow V \rightarrow V' P_1$  with  $V' \rightarrow P_2 \gamma$  ( $V, V' = \rho, \omega, \phi$  and  $P_{1,2} = \eta, \pi^0$ ).

## References

- [1] E. Klempt and A. Zaitsev, Physics Reports 454 (2007) 1;  
D. V. Bugg, Physics Reports 397 (2004) 257;  
C. Amsler and N. A. Törnqvist, Physics Reports 389 (2004) 61;  
F. E. Close and N. A. Törnqvist, J. Phys. G: Nucl. Part. Phys. 28 (2002) R249.
- [2] M. D. Scadron et al., Phys. Rev. D 69 (2004) 014010.



- [3] R. L. Jaffe, Phys. Rev. D 15 (1977) 267;  
R. L. Jaffe, Physics Reports 409 (2005) 1;  
L. Maiani et al., Phys. Rev. Lett. 93 (2004) 212002;  
G. 't Hooft et al., Phys. Lett. B 662 (2008) 424.
- [4] J. Weinstein and N. Isgur, Phys. Rev. Lett. 48 (1982) 659;  
J. Weinstein and N. Isgur, Phys. Rev. D 41 (1990) 2236;  
Yu. S. Kalashnikova et al., Eur. Phys. J. A 24 (2005) 437.
- [5] KLOE Collaboration, A. Aloisio et al., Phys. Lett. B 536 (2002) 209.
- [6] SND Collaboration, M. N. Achasov et al., Phys. Lett. B 479 (2000) 53;  
CMD-2 Collaboration, R. R. Akhmetshin et al., Phys.Lett. B462 (1999)380.
- [7] KLOE Collaboration, F. Ambrosino et al., Eur. Phys. J. C 49 (2007) 473;  
KLOE Collaboration, F. Ambrosino et al., Phys. Lett. B 634 (2006) 148;  
KLOE Collaboration, A. Aloisio et al., Phys. Lett. B 537 (2002) 21.
- [8] KLOE Collaboration, M. Adinolfi et al., Nucl. Instr. and Meth. A 488 (2002) 51;  
KLOE Collaboration, M. Adinolfi et al., Nucl. Instr. and Meth. A 482 (2002) 364;  
KLOE Collaboration, M. Adinolfi et al., Nucl. Instr. and Meth. A 492 (2002) 134.
- [9] KLOE Collaboration, F. Ambrosino et al., Nucl. Instr. and Meth. A 534 (2004) 403.
- [10] C. Amsler et al., Phys. Lett. B 667 (2008) 1.
- [11] N. N. Achasov and V. N. Ivanchenko, Nucl. Phys. B 315 (1989) 465;  
N. N. Achasov and A. V. Kiselev, Phys. Rev. D 68 (2003) 014006.
- [12] N. N. Achasov and V. V. Gubin, Phys. Rev. D 63 (2001) 094007.
- [13] G. Isidori et al., JHEP 0605 (2006) 049.
- [14] S. M. Flattè, Phys. Lett. B 63 (1976) 224.
- [15] A. Bramon et al., Phys. Lett. B 283 (1992) 416.
- [16] G. D'Agostini, Nucl. Instr. and Meth. A 362 (1995) 487.
- [17] KLOE Collaboration, F. Ambrosino et al., Phys. Lett. B 648 (2007) 267.